Proceedings of the ASME 2010 3rd Joint US-European Fluids Engineering Summer Meeting and
8th International Conference on Nanochannels, Microchannels, and Minichannels
FEDSM-ICNMM2010
August 1-5, 2010, Montreal, Canada

FEDSM-ICNMM2010-30551

BUBBLE FORMATION ON TOP OF SUBMERGED NEEDLE AND SUBSTRATE PLATES

Saeid Vafaei
School of Engineering and Materials Science, Queen Mary University of London
London, UK.

Panagiota Angeli
Department of Chemical Engineering, University College London
London, UK.

Dongsheng Wen
School of Engineering and Materials Science, Queen Mary University of London
London, UK.

ABSTRACT

The purpose of this investigation is to conduct a comparative study on the formation of bubble on top of a stainless steel needle nozzle and two substrate plate nozzles. The experimental study is conducted on a submerged needle nozzle with internal diameter of 0.51 mm and 0.155 mm thickness, and two stainless steel substrate plates with nozzle diameter of 0.4 mm and 0.51mm respectively. The experiment is carried out under low gas flow rates (0.015 ~ 0.85 ml/min). The bubble formation is recorded by a high speed video camera and detailed characteristics of bubble formation such as the variations of instantaneous contact angles, bubble heights and the radii of contact lines are obtained, which show a weak dependence on the flow rate under the conditions of current work. Using experimentally captured values of the height of bubble and the radius of contact line, the Young-Laplace equation is solved, which is found to be able to predict bubble evolution quite well until the last milliseconds before the detachment. Interestingly, it is found that the trends of the variation of bubble volume expansion rate from the stainless steel needle and the substrate plate are different, however, the rest of bubble characteristics such as radius of contact line, bubble height, contact angle, and radius of curvature of bubble apex follow same trends as the time and bubble volume change for formation of bubble on top of needle and substrate nozzles. A force analysis of bubble formation reveals that the observed variations of contact angles and other characteristics during the bubble growth period are associated with the relative contribution of surface tension, buoyancy and gravitational forces.

INTRODUCTION

The dynamics of bubble formation and bubble departure volume play a significant role in various applications involving dispersion of gas bubbles in liquids. The formation of bubbles on top of an orifice is a complicated phenomenon that can be affected by many parameters such as gas flow rate, orifice diameter and the depth of orifice in the liquid, liquid and gas physical properties, wettability and contact angle hysteresis [1-3].

Among many other studies, Wang *et al* [4] investigated the variation of contact angles for bubble formation from two immiscible fluids on top of a 0.5 mm diameter stainless steel pipe. The work was on drop formation in another immiscible liquid. Tsuge *et al* [5] investigated the effect of gas chamber volume, physical properties of gas, gas flow rate and orifice diameter on bubble formation phenomena from a submerged orifice. Flow through an orifice is mainly proportional to orifice diameter and growth period of the bubble. At low gas flow rates, the bubble volume is directly proportional to orifice diameter [6, 7], however at higher flow rates, bubble volume is reported to be a strong function of orifice diameter [8]. Marmur *et al* [9-10] theoretically studied the effect of chamber volume, orifice radius, orifice submergence and contact angle on quasi-static formation of bubble.

The Young-Laplace equation has been solved to predict the shape of axisymmetric liquid pendants and sessile drops on some ideal solid surfaces [11-13]. The predictions of Young-Laplace equation has been compared with experiments [11-14] and numerical solutions of the momentum and continuity equations by the volume of fluid method (VOF) [15]. For gas bubble formation, Gerlach *et al* [16] solved numerically the Young-Laplace equation by a force balance method in the

Cartesian coordinates to predict the bubble shape from millimeter-sized nozzles where good agreement with experiments was obtained. However extreme care is needed to solve the differential equations in Cartesian coordinates due to the singularity problem at the bubble apex. Attempts here will be on the prediction of gas bubble formation based and comparing it with our experimental results.

Most of the above mentioned work has been conducted on nozzles constructed on plain plates. Few studies have investigated the detailed characteristics of bubble formation on sub-millimeter nozzles where a departure from conventional-sized nozzle is expected to occur. Aiming to fill the gap, a comparative study will be conducted of bubble formation on top of a 0.51 mm submerged nozzle and of a substrate plate with the same orifice size at relatively low gas flow rates. Details of the bubble formation process such as the variation of instantaneous contact angle, radius of contact line, radius at bubble apex, and bubble height under different flow rate conditions will be revealed through a high-speed video camera. The experimental results will be compared against an analytical model where the influence of different forces on bubble formation will be revealed.

EXPERIMENTAL SETUP

Figure 1 shows a schematic diagram of the experimental system. It includes a gas supply system, camera and microscope, stainless steel nozzles and a gas flow rate controller. The nozzles are made of standard stainless steel needles and substrate. The internal diameter and thickness of a standard needle G21 is respectively 0.51 mm and 0.155 mm. The dimension and shape of the stainless steel substrate plate is given in Figure 2. The stainless steel substrate is polished (Ra 0.021 with Rz of 0.03 μm) after manufacture. The nozzles (needle or substrate) are submerged into a transparent square-sized glass container with size 20 by 20 mm and height 72 mm. The glass container is filled with quiescent deionized water to a height of 20 mm and open to the atmosphere under ambient conditions. Similar fittings and connections are used to connect the air supply in both the needle or substrate nozzles. The air flow is supplied from a pressurized air cylinder through a pressure reduction valve and flows vertically into the orifice. The flow rate is controlled by a flow controller in the range of 0.015-0.83 ml/min. The flow controller has a specified accuracy of $\pm 0.5\%$ of the nominal reading (model F-200CV-002 of Bronkhorst). A high speed camera (1200 frame/sec) and an optical microscope head are used to capture the images of bubble formation. The microscope setup is horizontal. The images are stored in a computer. Bubble height and the radius of contact line are measured in every image captured and are used as the two boundary conditions to solve the Young-Laplace equation numerically.

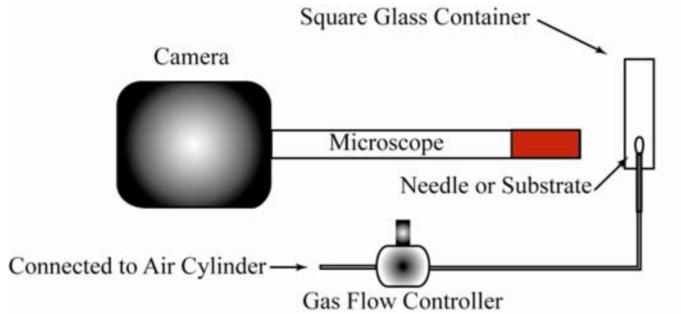

Figure 1 Schematic of the experimental setup.

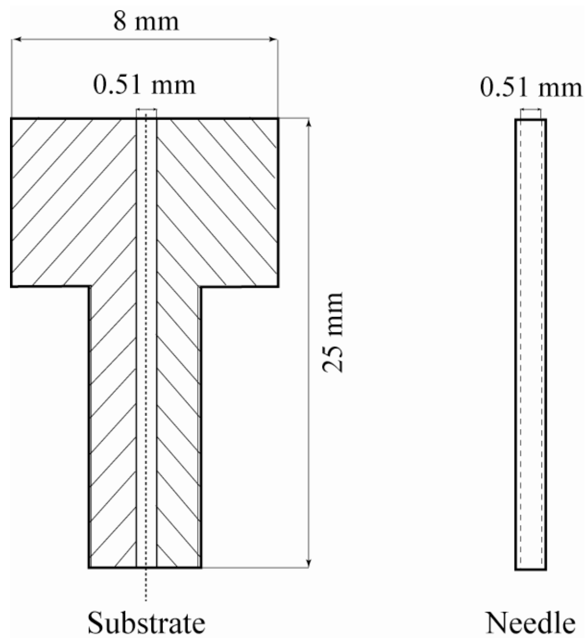

Figure 2 Dimensions of stainless steel substrate and needle.

PREDICTION OF AXISYMMETRIC BUBBLE FORMATION

It is assumed that bubble that formation because of very low flow rates is quasi equilibrium and at every time step equilibrium is achieved. The Young-Laplace equation represents a mechanical equilibrium condition between two fluids separated by an interface and can be written as

$$\Delta p = (\frac{1}{R_1} + \frac{1}{R_2})\sigma_{lg} \qquad (1)$$

where R_1 and R_2 are the radii of curvature, i.e. R_1 is the radius of curvature describing the latitude as the bubble rotates and R_2 is the radius of curvature in a vertical section of the bubble describing the longitude as it rotates. The center of R_1 and R_2 are on the same line but at different locations. Δp is the pressure difference between the gas, p_g, (see Figure 3) and liquid phase, p_l, which can be written as

$$p_g(z) = \frac{2\sigma_{lg}}{R_o} + P_o + \rho_g g z + \rho_l g h \quad (2)$$

$$p_l(z) = P_o + \rho_l g(h+z) \quad (3)$$

$$R_1 = ds/d\theta \text{ and } R_2 = r/\sin\theta \quad (4)$$

where R_o is the radius of curvature at apex and P_o is the ambient pressure, h is the hydrostatic head and θ is the contact angle at point *z*. Substituting equations (2-4) into equation (1), the Young-Laplace equation is written as

$$\frac{d\theta}{ds} = \frac{2}{R_o} - \frac{gz}{\sigma_{lg}}(\rho_l - \rho_g) - \frac{\sin\theta}{r} \quad (5)$$

The Young-Laplace equation can be solved, with the following system of ordinary differential equations for axisymmetric interfaces, to obtain the bubble shape.

$$\frac{dr}{ds} = \cos\theta \quad (6)$$

$$\frac{dz}{ds} = \sin\theta \quad (7)$$

$$\frac{dV}{ds} = \pi r^2 \sin\theta \quad (8)$$

This system of ordinary differential equations avoids the singularity problem at the bubble apex, since

$$\left.\frac{\sin\theta}{r}\right|_{s=0} = \frac{1}{R_o} \quad (9)$$

Knowing two parameters of the bubble shape (such as contact angle, radius of contact line, bubble volume, or location of the apex), the system of ordinary differential equations (5-8) can be solved to obtain the axisymmetric bubble shape, using the following boundary conditions [11].

$$r(0) = z(0) = \theta(0) = V(0) = 0 \quad (10)$$

In this calculation, the experimental values of the radius of contact line and height of bubble, which can be determined accurately from experiments, are used as the only two inputs to solve the Young-Laplace equation for each step time of bubble formation to predict parameters of the bubble.

The accuracy of measurement of radius of contact line and bubble height is 5 μm and percentage error of calculation is $\pm$ 1.5 μm.

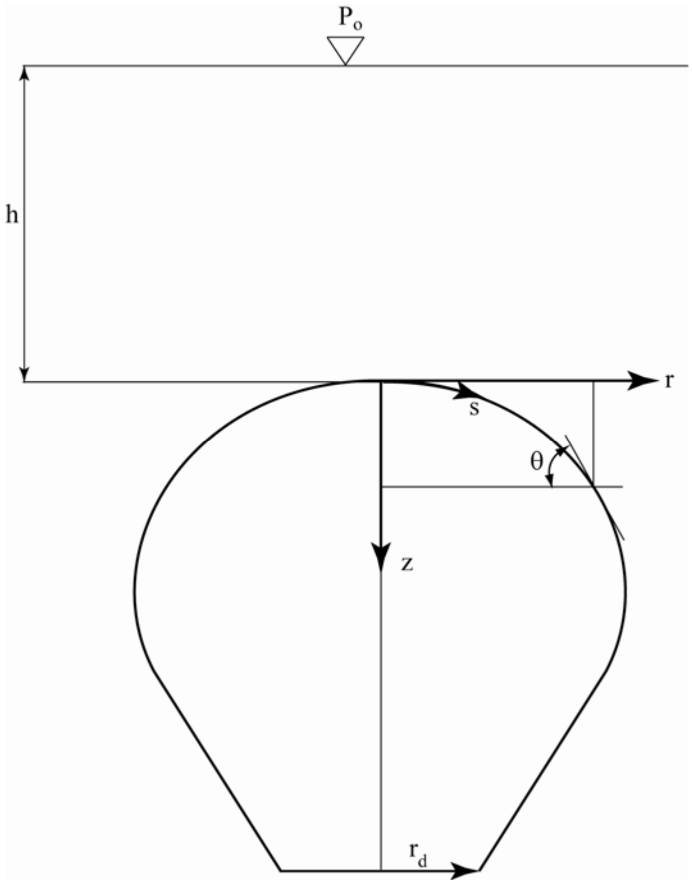

Figure 3. Schematics of an axisymmetric bubble.

The set of first-order differential equations are solved in Version 7 of Matlab environment using the 4th order Runge-Kutta method. Since the Young-Laplace equation can not predict the bubble volume at the last milliseconds, the bubble departure volume is calculated by summing the bubble volume at the last point that can be predicted by the Young-Laplace equation and the integral of gas flow rate at the last moments of the detachment, $\int_{t_l}^{t_d} Q dt$, t_d where is the detachment time obtained from experiment, and t_l is the last moment of the bubble formation that can be predicted by Young-Laplace equation.

FORCE ANALYSES

To understand better the mechanism of bubble formation from a needle or a substrate nozzle, the forces acting on the forming bubble are calculated. The main forces are: buoyancy force (upwards) = $(\rho_l - \rho_g)gV$; force due to the Laplace pressure (upwards) = $\frac{2\sigma_{\lg}}{R_o}\pi r_d^2$; hydrostatic force of the liquid phase (downwards) = $\rho_l g \delta \pi r_d^2$; the vertical component of the surface tension force (downwards) = $2\sigma_{\lg} r_d \pi \sin\theta_o$; and the downward inertial force = $\frac{d(MU)}{dt}$.

In general, the inertial force [17-19, 20-23] is given by

$$\frac{d(MU)}{dt} = M\frac{dU}{dt} + U\frac{dM}{dt} \qquad (11)$$

where M is the virtual mass of the bubble and can be written [17-18, 20] as

$$M = (\frac{11}{16}\rho_l + \rho_g)V \qquad (12)$$

U is the bubble velocity whose definition depends on the application. For instance when a bubble is detached and is moving upwards, U can be the velocity of the bubble centre [18], while when the bubble is attached the velocity is taken equal to the rate of bubble radius expansion assuming the bubble is spherical [22-23],. In this study since the bubble still attached to the nozzle, U is calculated from the change of bubble height, δ, with time [17, 19, 21, 24]

$$U = \frac{d\delta}{dt} \qquad (13)$$

Substituting equations (12) and (13) into (11), the inertial force is

$$\frac{d(MU)}{dt} = (\frac{11}{16}\rho_l + \rho_g)[V\frac{d^2\delta}{dt^2} + \frac{dV}{dt}\frac{d\delta}{dt}] \qquad (14)$$

RESULTS AND DISCUSSIONS

During the experiments, the high speed video camera captured details of the bubble formation process. Image processing provided accurate measurements of bubble parameters such as the radius of bubble contact line and the bubble height. Knowing the radius of contact line and height of bubble, the Laplace-Young equation is solved to predict the bubble shape. Figure 4 compares the theoretical prediction from the Young-Laplace equation with the experimental results for bubble evolution under a gas flow rate of 0.475 ml/min with the G21 needle nozzle. Good comparison was also found for the other gas flow rates used in this work (0.015-0.85 ml/min). Similar accuracy is observed for the prediction of bubble shape on top of stainless steel substrate with 0.4 mm and 0.51 mm orifice. The Young-Laplace equation is satisfied up to the detachment period, where the bubble has almost the maximum volume and would depart by supplying further gas amount or introducing small perturbations around the bubble. In the last milliseconds close to departure, the bubble is being stretched and consequently viscosity plays an important role. Such a good agreement before the bubble departure is expected for bubble formation

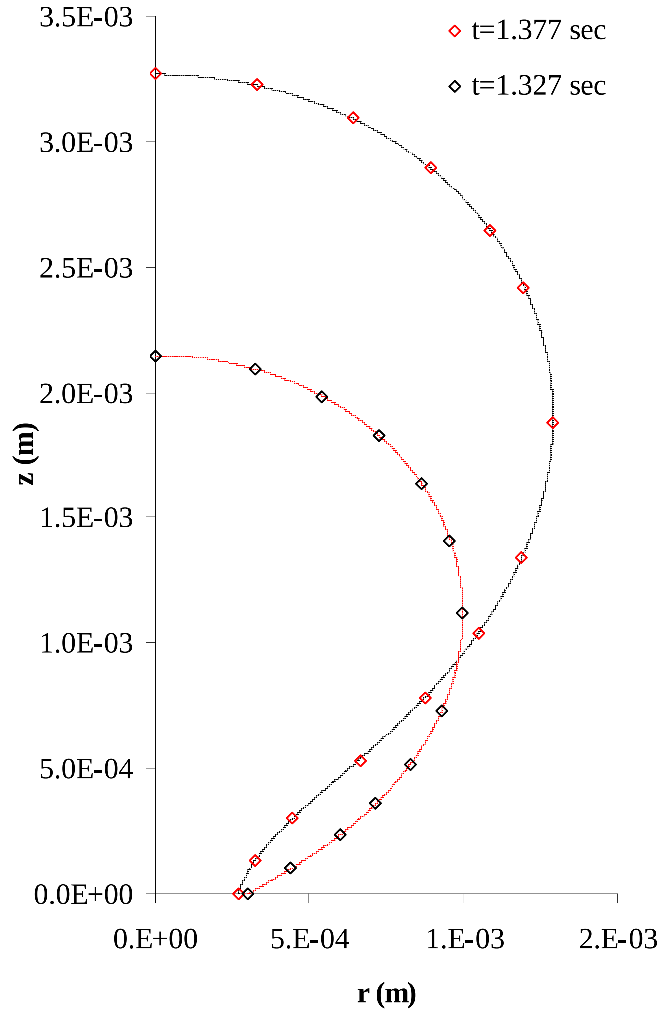

Figure 4. Comparison between experimental bubble shape and prediction of Young-Laplace equation for 0.475 ml/min gas flow rates on top of G21 needle nozzle. (Exp: Dotted points, Prediction: dash lines).

under low flow rate conditions as the gas-liquid shear stress becomes negligible. As gas flow rate increases, the increase of gas-liquid shear stress could invalidate the Young-Laplace equation. The increase of gas flow rate will increase the bubble generation frequency, which affects the formation of subsequent bubbles. Since the Young-Laplace equation was found to predict well the experimental data it was further used to calculate other characteristics of bubble formation such as bubble volume and the radius of curvature at apex that are difficult to determine accurately from experiments.

Changing nozzle size and form from needle to substrate for the same material will affect the formation of bubble, and departure bubble volume and consequently average gas flow rate, $Q_{av} = Vf$. V is detached bubble volume and f is bubble frequency.

Figure 5 shows the variation of the contact angle and bubble volume with time on top of stainless steel needle (G21) and substrate plate with 0.51 mm nozzle diameter. Initially, the contact angle decreases with bubble volume as long as the effect of buoyancy force is negligible. As bubble volume increases, the effect of buoyancy force becomes more effective and the contact angle start increasing with bubble volume. In the necking stage, the variation of bubble volume is not significant as it can be seen in Figure 5, however since the bubble is being stretched, the contact angle continues to increase. Figure 6 demonstrates the variation of radius of contact line and bubble height with time on top of stainless steel needle (G21) and substrate with 0.51 mm nozzle diameters; similar trends are found for both nozzles.

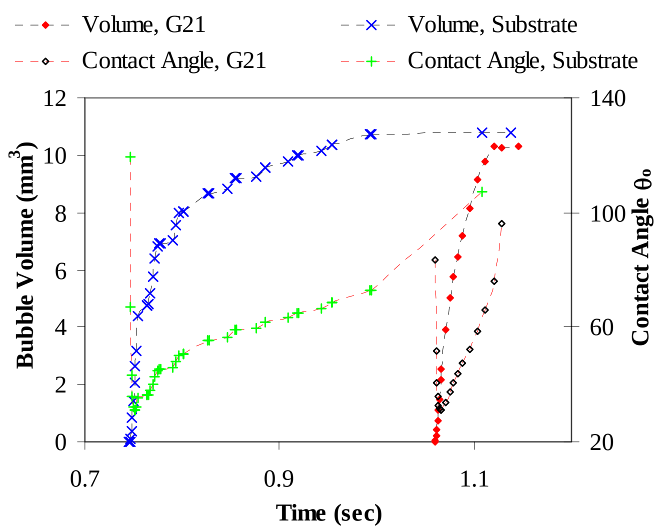

Figure 5. Variation of bubble volume and contact angle with time on top of a stainless steel needle (G21) and substrate with 0.51 mm nozzle diameter for 0.545 ± 0.015 ml/min gas flow rates.

In Figure 7 the variation of contact angle and radius of contact line with volume on top of stainless steel needle (G21) and substrate plate for 0.51 mm nozzle diameters can be seen. As bubble volume increases, the radius of contact line increases. At the same time the contact angle decreases (bubble is pushed outwards on the substrate). Once the effect of buoyancy becomes considerable, the entire bubble will move upwards and consequently the radius of contact line will start to decrease, and the contact angle start being increased.

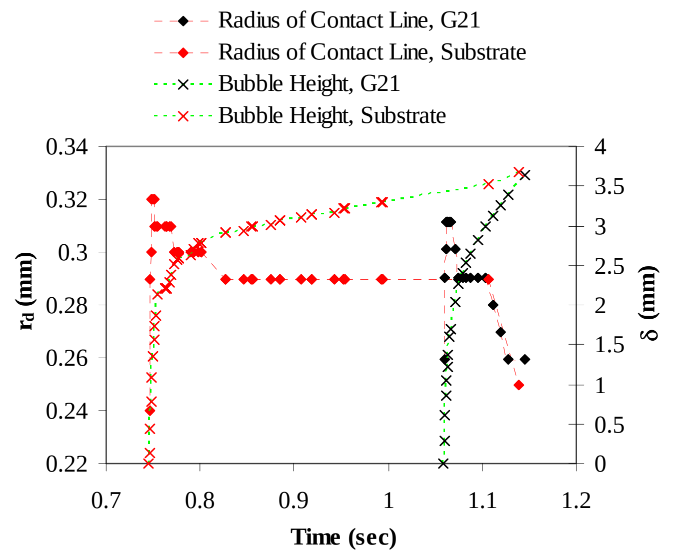

Figure 6. Variation of radius of contact line and bubble height with time on top of a stainless steel needle (G21) and substrate with 0.51 mm nozzle diameters for gas flow rate of 0.545 ± 0.015 ml/min.

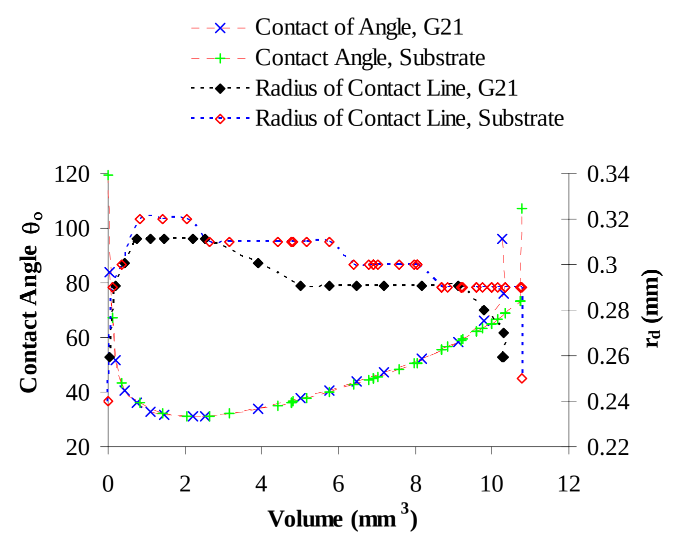

Figure 7. Variation of contact angle with bubble volume on top of a stainless steel needle (G21) and substrate with 0.51 mm nozzle diameters.

The radius of contact line goes to a maximum as bubble volume increases. This maximum radius of contact line is controlled by the balance of acting forces at the triple line. It is clear that the variation of contact angle for a given bubble volume is not much dependent on the nozzle configuration. Furthermore, the trend of the variation of the radius of contact line with volume on top of a needle or substrate nozzles is almost the same. In general, the trends of variation of bubble characteristics with time and volume are the same for both nozzle configurations.

However detailed analysis shows that there are notable differences on the rate that bubble characteristics change with time, for bubbles forming on top of needle and substrate nozzles, as shown in Figures 8 and 9 respectively. In case of the formation of bubble on top of a stainless steel needle, the bubble volume expansion rate increases at the beginning to a maximum and then decreases monotonically with further increase of bubble volume, until bubble detachment. However, the rate acquires a periodic form for formation of bubble on top of a stainless steel substrate plate of the same nozzle size. At the early stage of the bubble formation, i.e. $V \prec 2mm^3$, the bubble volume expansion rate increases rapidly to the maximum value in a similar way as from a submerged nozzle. However after that peak in the rate, further increase of the bubble volume reduces the growth rate, to nearly a zero value at $V \approx 4.7mm^3$. The phenomenon is repeated several times until the final departure of the bubble at $V \approx 10.7mm^3$. The peak value and the period of these cycles reduce as bubble grows. These cyclic fluctuations are almost independent of the average gas flow rate. At the moment, the causes of this behavior are still unknown. Detailed investigations are currently ongoing. It is also observed in the experiments that as the nozzle diameter of the stainless steel substrate plate decreases, the frequency of fluctuation of bubble volume expansion rate decreases (less number of peak). The Laplace-Young equation is found out to be invalid at the time when the bubble volume expansion rate is around zero value, but the Laplace-Young equation predicts the bubble shape quite well at the zero bubble volume expansion rates, and all the other bubble growth period. Figure 8 and Figure 9 shows only the valid points by Laplace-Young equation.

The variation of the major forces with time can be seen in Figure 10 for both nozzles with 0.51 mm diameter. The trends of the variation of the forces are similar for the needle and the substrate nozzles. At the initial stages (t=746.516-751.514 ms) of the bubble formation, the buoyancy force is negligible since the bubble volume is small. As the bubble grows the radius of curvature at the apex increases and therefore the force due to Laplace pressure decreases. At the same time the bubble volume expansion rate and the downward inertial force increase. Since the buoyancy force is still not effective, and the inertial force increases rapidly, the bubble expands more in the lateral direction, so the radius of contact line increases and the contact angle decreases (see Figure 7). Even though that radius of contact line increases, the reduction in contact angle has a larger effect and the vertical component of surface tension force decreases. Once the inertia force reaches its maximum (t=749.848 ms), the bubble volume expansion rate starts to decrease and so is inertial force. With a further increase in the bubble volume (749.848-1138.217 ms), the buoyancy force increases and lifts the bubble away from the nozzle opening. This bubble movement increases the contact angle and the vertical component of surface tension. Eventually the buoyancy force increases sufficiently to bring the bubble to the necking stage and departure from the nozzle (t=1138.217 ms).

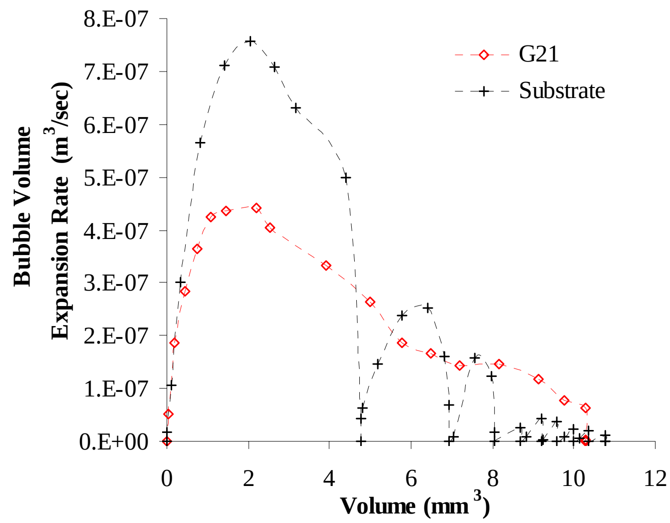

Figure 8. Variation of bubble volume expansion rate with volume on top of a stainless steel needle (G21) and substrate with 0.51 mm nozzle diameters for 0.545 $\pm$ 0.015 ml/min gas flow rates.

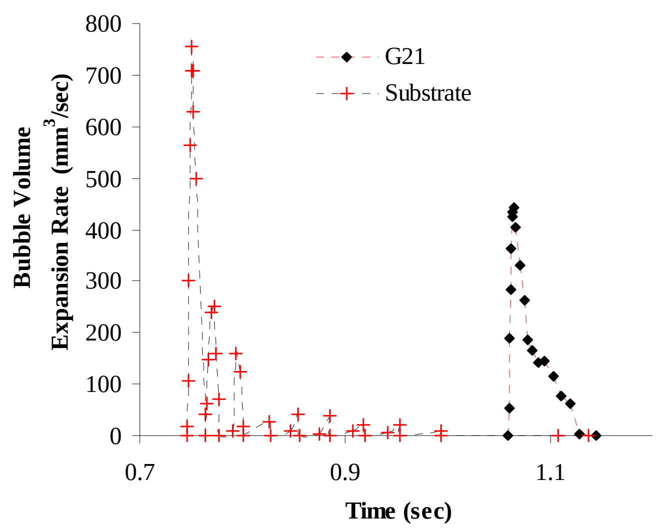

Figure 9. Variation of bubble volume expansion rate with time on top of a stainless steel needle (G21) and substrate plate of 0.51 mm nozzle diameters for 0.545 $\pm$ 0.015 ml/min gas flow rates.

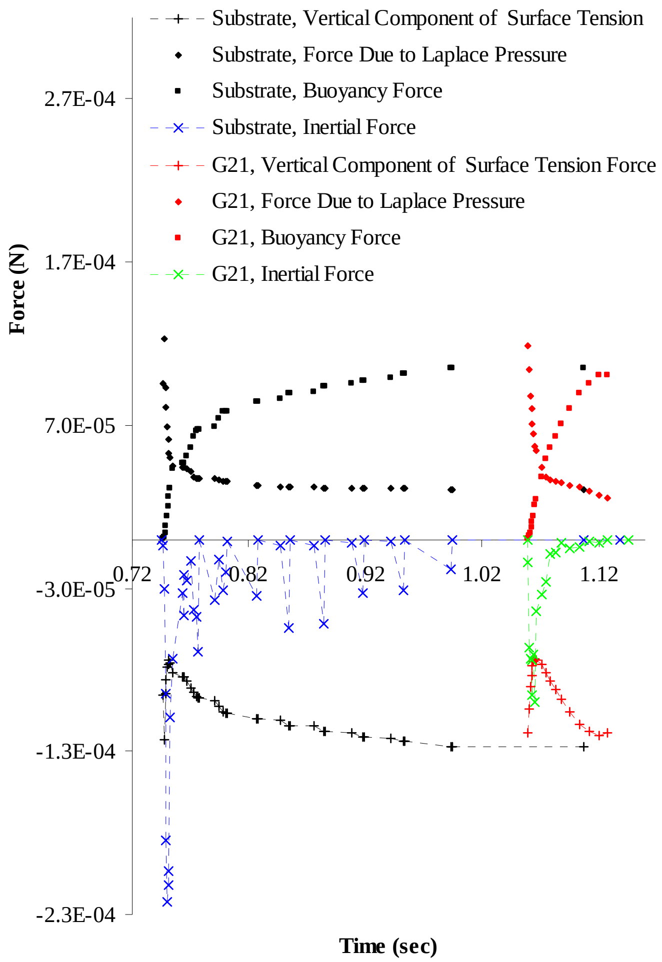

Figure 10. Variation of major forces acting through bubble growth, forming on top of stainless steel needle and substrate nozzles with same internal diameter (0.51 mm). The nominal gas flow rate is 0.5 ml/min.

The relative importance of forces together with the large bubble expansion rates at the initial stages of bubble formation may be able to explain the fluctuations on the expansion rate for bubbles forming from a substrate nozzle. The high initially bubble volume expansion rate increases the downward inertial force rapidly (see Figure 10) which reaches a maximum within 3.33 milliseconds (almost 0.85 % of bubble formation time). This large increase in inertial force rapidly pushes the air bubble downwards, possibly compresses the air and causes the fluctuations seen. The maximum inertial force for a bubble on top of a substrate nozzle is almost twice the one on top of the needle nozzle. The downward inertial force in the case of a needle increases from zero to maximum within 5.83 milliseconds (almost 6.79 % of bubble formation time). As the magnitude of the inertial force is less than in the substrate case and its increase occur over a longer period of time, no fluctuations are observed.

CONCLUSIONS

This work investigated fundamentally the formation of air bubbles on submerged stainless steel needle or substrate nozzle under very low flow rate conditions (0.015 ~ 0.85 ml/min). Detailed characteristics of bubble formation are recorded by a high speed camera and compared with an analytical model. Specific conclusions can be drawn including:

1) The nozzle form (needle or substrate plate) will affect the variation of rate of bubble characteristics, but not the trend of variation of bubble characteristics. In general, the trends of variation of bubble characteristics with time and volume are the same for formation of bubble on top of the stainless steel needle and substrate plate.

2) Large differences in bubble volume expansion rate are observed for bubbles forming on top of needle and substrate plate nozzles. A unique cyclic fluctuation of bubble expansion rate is observed for the substrate plate case, which is dependent on substrate plate nozzle diameter, but not much on gas flow rate.

Using experimentally captured values of bubble height and radius of contact line, the Young-Laplace equation is found to be able to predict the bubble evolution quite well except a few characteristic points around the zero volume expansion rates and the detachment points.

NOMENCLATURE

f	Bubble Frequency $[Hz]$
g	Acceleration of gravity $[m/s^2]$
V	Bubble Volume $[m^3]$
p_g	Gas pressure $[Pa]$
p_l	Liquid pressure $[Pa]$
Q	Gas flow rate $[m^3/s]$
R_o	Radius of curvature at origin $[m]$
R_1, R_2	Radius of curvature $[m]$
r_d	Radius of contact line of droplet $[m]$
s	Curve length $[m]$
t_d	Detachment time $[s]$
t_l	Last moment of bubble formation, predicted by Young-Laplace equation $[s]$

Greek Symbols

δ Height of bubble $[m]$

θ_o Contact angle [*Deg.*]

ρ_l Liquid density $[kg/m^3]$

ρ_g Gas density $[kg/m^3]$

$\sigma_{\lg}$ Bulk liquid -gas surface tension

ACKNOWLEDGMENTS

The authors are grateful for the financial support of EPSRC under the grant number EP/E065449/1.

REFERENCES

[1] R. Kumar, N.R. Kuloor, Advances in Chemical Engineering 8 (1970) 255.

[2] S. Gnyloskurenko, A. V. Byakova, O.I. Raychenko, T. Nakamura, Colloids and Surfaces A: Physicochemical and Engineering Aspects 218 1-3 (2003) 73.

[3] W. Fan, S. Jiang, C. Zhu, Y. Ma, H. Li, Optics and Laser Techbology 40 (2008) 389.

[4] W. Wang, K. H. Ngan, J. Gong, P. Angeli, Colloids and Surface A: Physicochem. Engineering Aspects 334, (2009) 197.

[5] H. Tsuge, S. I. Hibino, Chemical Engineering Communications, 22 (1983) 63.

[6] R. L. Datta, D.H. Napier, D.M. Newitt, Transactions of the Institution of Chemical Engineers 28 (1950) 14.

[7] R. L. Benzing, J. E. Myers, Ind. Eng. Chem, 47 (1955) 2087.

[8] C. J. Quigley, A. I. Johnson, B. L. Harris, Chemical Engineering Progress Symposium Series, S1 (1955) 31.

[9] A. Marmur, E. Rubin, Chemical Engineering Science 28 (1973) 1455.

[10] A. Marmur, E. Rubin, Chemical Engineering Science 31 (1976) 453.

[11] A.W. Neumann, J.K. Spelt, Applied Surface Thermodynamics, M. Dekker, 1996.

[12] O.I. del Rio, A.W. Neumann, Journal of Colloid and Interface Science 196 2 (1997) 136.

[13] S. Vafaei, M.Z. Podowski, Advances in Colloid and Interface Science 113 2-3 (2004) 133.

[14] D. Gerlach, G. Biswas, F. Durst, V. Kolobaric, International Journal of Heat and Mass Transfer 48 2 (2005) 425.

[15] D. Gerlach, G. Tomar, G. Biswas, F. Durst, International Journal of Heat and Mass Transfer 49 (2006) 740.

[16] D. Gerlach, G. Biswas, F. Durst, V. Kolobaric, International Journal of Heat and Mass Transfer 48 (2005) 425.

[17] H. Tsuge, S. I. Hibino, Chemical Engineering Communications, 22 (1983) 63.

[18] A. A. Kulkarni, J. B. Joshi, Industrial & Engineering Chemistry Research, 44 (2005) 5873.

[19] M. Martin, F. J. Montes, M. A. Galan, Chemical Engineering Science, 61 (2006) 5196.

[20] R. Kumar, N. R. Kuloor, Advances in Chemical Engineering 8 (1970) 255.

[21] M. Martin, F. J. Montes, M. A. Galan, Chemical Engineering Science, 61 (2006) 363.

[22] S. Ramkrishnan, R. Kumar, N. R. Kuloor, Chemical Engineering Science 24 (1969) 731.

[23] A. Satyanarayana, R. Kumar, N. R. Kuloor, Chemical Engineering Science 24 (1969) 749.

[24] K. Terasaka, H. Tsuge, Chemical Engineering Science 48 (1993) 3417.

